A Compact 4G MIMO Antenna Integrated with a 5G Array for Current and Future Mobile Handsets

Rifaqat Hussain, Ali T. Alreshaid, Symon K. Podilchak and Mohammad S. Sharawi

Abstract

A novel integrated antenna solution for wireless handheld devices is proposed for the existing 4G standards and upcoming 5G systems for broadband, high data rate communications. The complete antenna system is a unique combination of a multiple-input-multiple-output (MIMO) antenna system at microwave frequencies and a millimeter(mm)-wave antenna array. The MIMO antenna system consists of two reactive loaded monopoles while the mm-wave array consists of a planar 2 by 4 slot antennas. The integrated antenna system covers the frequency bands from 1870 to 2530 MHz for 4G standards along with the upcoming 5G mm-wave band at 28 GHz. In addition, the integrated antenna system is planar and is designed for typical smart phone devices with a standard 60 mm by 100 mm by 0.965 mm back plane. Excellent field correlation values were obtained across the 4G band while realized peak gain values of 4 dBi and 8 dBi were respectively measured for the MIMO and mm-wave antenna arrays. The proposed antenna design may also be useful for other compact implementations that support 4G and 5G communications.

Keywords: MIMO, wide-band antenna, mm-wave antenna array, integrated 4G/5G antenna

I. Introduction

Exponential growth in data rate requirements triggered by new smart wireless devices brings significant changes in setting new wireless standards for communication systems. Long term evolution (LTE), broadband LTE services, and 4G commercial services are adopted in modern wireless standards to meet such high data requirements. After LTE commercialization, industry and academic researchers started focusing on next generation broad-band wireless and mobile communications for future 5G wireless networks. These systems gained popularity recently and wireless devices complying with such 5G standards should be able to operate with intensive data processing capability and high system throughput. This upcoming wireless standard requires large bandwidth (BW) and hence utilizes the millimeter(mm)-wave spectrum for multi-Gbps throughput [1]. The prospective 4G/5G integrated communication environment is shown in Figure 1 for current and future mobile devices.

R. Hussain, A. T. Alreshaid and M. S. Sharawi are with the Electrical Engineering Department, King Fahd University for Petroleum and Minerals (KFUPM), Dhahran, 31261 Saudi Arabia, email:{*rifaqat, alreshaid, msharawi*}*@kfupm.edu.sa*.

S. Podilchak is with the Royal Military College of Canada (RMC) and with the Institute of Sensors, Signals and Systems (ISSS) within the School of Engineering and Physical Sciences (EPS) at Heriot-Watt University, Edinburgh, Scotland, United Kingdom EH14 4AS, email: *skp@ieee.org*

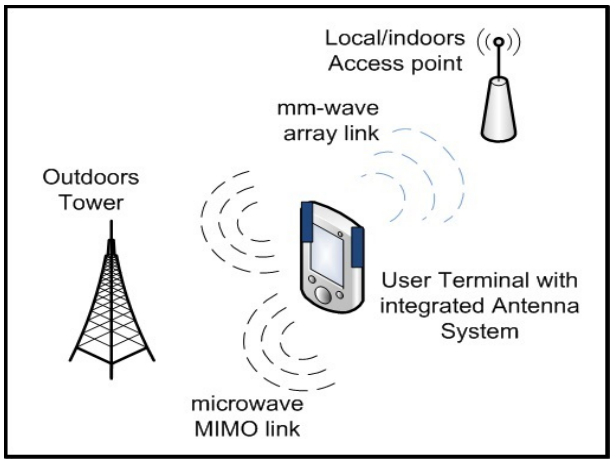

Figure 1: Microwave and mm-wave wireless communication scenario for current and future mobile devices.

One of the major technologies that can enhance data throughput in 4G networks is multiple-input-multiple-output (MIMO) systems. This requires the use of multiple antennas and these systems require MIMO characterization, and as such, multiple antenna evaluations are equally important when compared to more conventional metrics such as input matching, operational frequency, and antenna gain [2], [3].

Several antenna designs complying with 4G standards were presented such as in [4]–[7] for wireless handheld devices. In [4] a wideband antenna was presented for the 4G LTE system. The frequency bands covered were 1.76 to 2.68 GHz, including PCS, UMTS/LTE, Bluetooth, ISM, and WLAN bands. The single element was circular in shape with a radius of 50 mm. Its large size made it difficult to accommodate more antenna elements in a MIMO configuration within small wireless handheld devices. An LTE mobile handset antenna was presented in [5] with single element dimensions of 15 mm by 40 mm. The two frequency bands covered by this design were 698 to 960 MHz and 1710 to 2690 MHz. In [6], a dual-band monopole antenna for WiFi and 4G LTE applications was presented. The dimensions of the given antenna were 41.6 mm by 28.38 mm by 1.52 mm. The two frequency bands covered were 2.3 to 3.0 GHz and 4.7 to 5.9 GHz. In [7], two different single element slot meander patches were presented complying with 4G LTE standards. The frequency bands covered were 1.68 to 3.88 GHz for the first antenna, while the second multi-band antenna covered three frequency bands 0.5 to 0.75 GHz, 1.1 to 2.7 GHz, and 3.3 to 3.9 GHz. The total dimensions of the antenna system was 100 mm by 35 mm by 1.635 mm. Also, the LTE 4G antennas presented in [4]–[7] were either complicated in structure or with large dimensions and thus integration into a compact MIMO configuration for small handheld devices and mobile terminals could be challenging.

MIMO antenna elements for 4G standards were further presented in several references such as [8]–[13]. In [8], a two element PIFA antenna was presented for WLAN and LTE bands. The frequency bands covered were 2.1 to 2.9 GHz with single element dimensions of 10 mm 40 mm by 20 mm. A non-planar MIMO antenna was also presented in [9]. The design was a combination of a monocone and a microstrip antenna. The design was fabricated

on a circular board with a radius equal to 126 mm and height 39.15 mm. The presented design offered connectivity between 750 to 2730 MHz covering several well-known frequency bands. A MIMO dielectric resonator antenna for LTE applications was also presented in [10]. Two orthogonal modes of the antenna were excited by using a coplanar waveguide and a coaxial probe feed mechanism. The two frequency bands achieved were 2.09 to 3.38 GHz and 2.40 to 3.09 GHz, respectively. The dimensions of board used were 70 mm by 70 mm by 11.60 mm. In [11]–[13], frequency reconfigurable antennas were also presented covering several well known LTE bands. The given antenna designs were compact and suitable for MIMO operation in wireless handheld devices complying with 4G standards. The dimensions of the boards used were typically 65 mm by 120 mm.

To continue these efforts researchers started developing different antenna designs to be used in handheld devices after announcing the 28 GHz band was a candidate for the upcoming 5G standard for cellular networks [14], [15]. A complex mesh-grid antenna array with 16 radiating elements was proposed in [16]. The achieved bandwidth (BW) by the system was almost 3 GHz with a gain of 10.9 dBi. Although the size of such a structure was small (placed at the edge of a phone), the mesh structure is considered a complex multi-layered via based design, and this work did not show the feeding network for such a mesh array along with its accompanying losses or a prototype to compare against.. In [17], a BW of 2.85 GHz was achieved using a patch antenna, which was mounted on a Low Temperature Co-fired Ceramic (LTCC) structure. In addition, good behavior was noted in [18], where a tapered slot antenna array was fed by a surface integrated waveguide. The BW in that work was as high as 10 GHz with a gain of 14.5 dBi.

In this paper we propose a novel integrated antenna system that will be a viable solution for both 4G and the upcoming 5G standards. The antenna structure is a unique combination of a microwave MIMO antenna system along with a mm-wave slot antenna array for high gain when considering short range data links. The integrated structure could be utilized in 4G wireless networks covering several well-known frequency bands from 1870 to 2530 MHz along with the mm-wave frequency band at 28 GHz. To the authors' knowledge none of the reported designs found in the literature are able to provide such a novel integrated antenna system.

The design procedure for our proposed 4G/5G antenna system is provided and measurement results are reported along with full MIMO antenna characterization. Also, our proposed wide-band MIMO antenna system and the mm-wave antenna array are compact and are fabricated on a fractional area of a typical smart phone size. The total printed circuit board area occupied by the design is 60 mm by 30 mm by 0.965 mm on a standard mobile phone back plane of 60 mm by 100 mm by 0.965 mm.

The rest of the paper is organized as follows. Sections II describes the antenna system design for both the MIMO antenna and the mm-wave antenna array. The simulation and measurement results are given in Section III while some conclusions are provided in Section IV.

II. Antenna System Design

The proposed integrated microwave MIMO antenna system along with the mm-wave antenna array and its feed network are shown in Figure 2(a). The complete antenna system is a multi-layer design placed on a 60 mm by 100 mm by 0.965 mm backplane. Four layers are used in our planar design, and thus by proper placement of the recessed ground plane and orientation of the mm-wave antenna array, good MIMO operation is possible for the two 4G antennas. In particular, the ground plane layer acts as a clever co-planar reflector for the two MIMO antennas enabling beam tilting, and is sandwiched between the two dielectric layers (top that is holding the MIMO antennas and bottom holding the mm-wave feed network). This ground plane is also adhered to the top layer by a bonding material with a thickness of 0.05 mm and a relative dielectric constant (ϵ_r) of 2.94. Further design details of the two antenna systems are given in the following sections.

The fabricated model of the proposed design is reported in Figure 2(b). Figure 2(b-i) shows the top view of the 2-element MIMO antenna system. Figure 2(b-ii) shows the bottom layer of the fabricated antenna system containing the feed network for the slot antenna array.

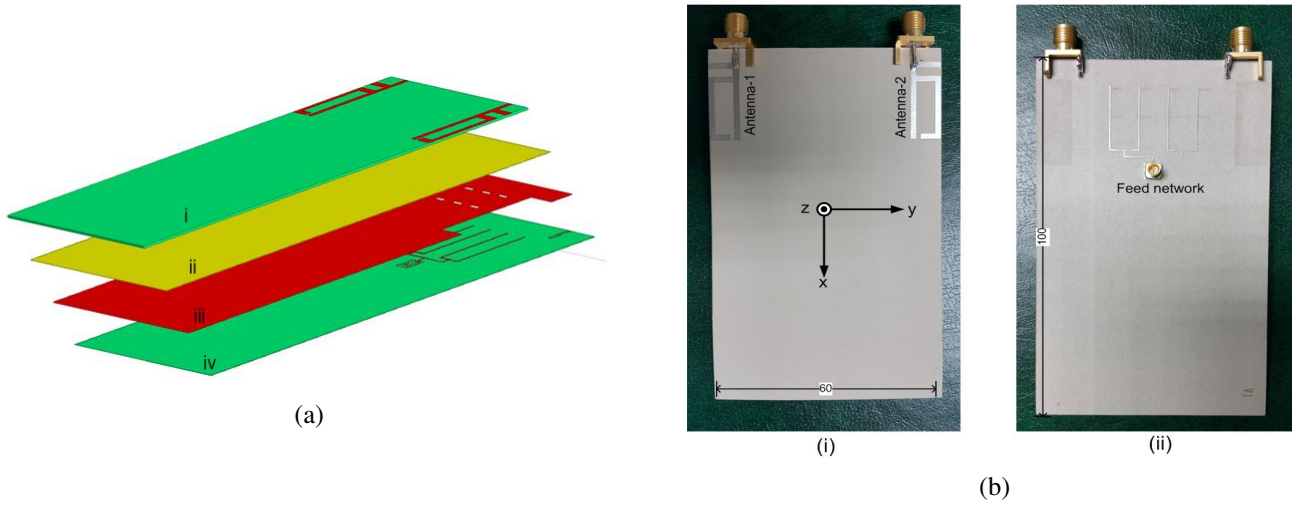

(a) (i) (ii) (b)

Figure 2: (a) Proposed integrated multi-layer antenna system: top layer (i), binding glue (prepreg) layer (ii), ground plane (iii), and bottom layer (iv). (b) Fabricated prototype. (i): Top view (see Fig. 2(a-i), top layer) and (ii): bottom view (see Fig. 2(a-iv), bottom layer). All dimensions in millimeters.

A. Operation of the MIMO Antennas

The design procedure for the single MIMO antenna element started with a simple microstrip monopole antenna operating at a higher frequency band than desired. The initial optimized design is shown in Figure 3(a-i) which was resonating at 2.925 GHz. Microstrip line stubs (as shown in red color in Figure 3(a-ii) were added to the optimized antenna structure (as shown in pink color in Figure 3(a-ii), for miniaturization and reactive loading to reduce the

resonance frequency to the desired 4G band (see Figure 3(a-ii)). HFSS^{TM} was further used for the optimization process. Parametric sweeps were also performed on various antenna parameters including the size of the gap between the two long radiating lengths. All three branches of the antenna were selected to increase the effective BW. Optimized dimensions of the final MIMO system are shown in Figure 4(a). The reflection coefficient curves for the antennas given in Figures 3(a-i) and 3(a-ii) are shown in Figure 3(b) as case A and case B, respectively.

The proposed antenna design was further studied by reducing the ground plane as shown in Figures 3(a-iii) and 3(a-iv) , respectively. The reflection coefficient curve of the given modified monopole design is also shown in Figure 3(b) as case C. The given antenna demonstrated a minimum in its reflection coefficient at 2.66 GHz and generated an omni-directional radiation pattern similiar to a monopole as can be observed in Figure 3(c) . Thus the proposed MIMO antennas are essentially a planar and compact monopole-like ones, with additional ground plane reflector sections complimented by the mm-wave antenna array, to enhance MIMO performance (the reflector is shown in the final configuration, see Figure 4(b)).

B. Integrated 4G MIMO Antenna

The proposed MIMO antenna system consists of a modified monopole antenna design as shown in Figure 4. The two elements were separated by a distance of 42 mm to be placed at the two top corners of the mobile device with single element dimensions of 7.9 mm by 25.4 mm. The MIMO elements were mounted on the top layer of the board as shown in Figure 4(a) while the ground plane of the proposed design is shown in Figure 4(b). The MIMO antennas were simulated and fabricated on a Rogers RO3003 board with ϵ_r = 3 , tanδ = 0.0013, and a thickness of 0.76 mm.

C. mm-wave 5G Antenna Array

Due to the high path loss at the 28 GHz mm-wave band, antenna arrays can be used to provide improved gain. Aiming at handheld devices, which mainly limit the size of the design due to the available real estate, a 2×4 antenna array was adopted in this work. Due to the structural advantages of the slot antenna, it is chosen to be the radiating element of the mm-wave antenna array. A half wavelength slot antenna is fed by a microstrip line of width 0.18 mm, which corresponds to 50-Ω via slot coupling. The feeding point was calculated and found to be 0.05 λ from one of the slot short edges. The material used for the substrate is also RO3003 with a thickness of 0.13 mm.

The design procedure of mm-wave antenna array was started with a corporate feed combiner/splitter design. The 2×4 antenna array is fed by four parallel microstrip lines separated by 7.5 mm, where each line is feeding two elements in series. The line widths of feed network were selected as 0.35 mm and 0.18mm corresponding to 70.7Ω and 50Ω, respectively. The lengths of the feeding arms from the splitter to the array as well as the small extension

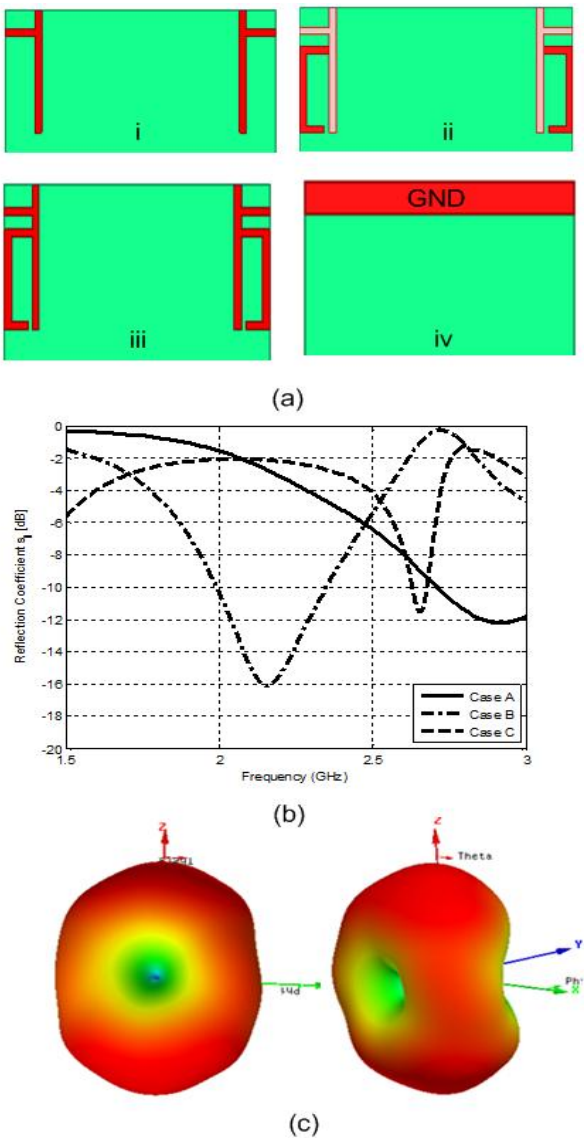

Figure 3: Design evolution of the MIMO antenna: case A (a-i), case B (a-ii), case C (a-iii), ground plane of antenna in case C (a-iv), corresponding reflection coefficient curves (b), and beam patterns of the case C (c). It should be mentioned that these results did not include the final ground plane or the mm-wave antenna array.

beyond the second slot were optimized for proper impedance matching. The delivered power at the each output port of the feed network without the array were approximately -6 dB as expected with same phase as shown in Figures 6(a) and 6(b). The second stage of mm-wave array was the design of slot antenna elements with a microstrip line feed coupling. The slot antenna was designed at 28 GHz corresponding to a wavelength of 7 mm on the RO3003 substrate used with 0.13mm thickness. The antenna was optimized with almost half-wavelength resonance with final dimension of 3.75mm by 0.75 mm. The feeding location was placed closer to the edge to provide matching to 50 Ω.

The orientation of the 4G, two-element MIMO antenna system with respect to the mm-wave slot antenna array is shown in Figure 4(c). A mini-smp connector (PE44489) was connected to the single feed of the mm-wave array.

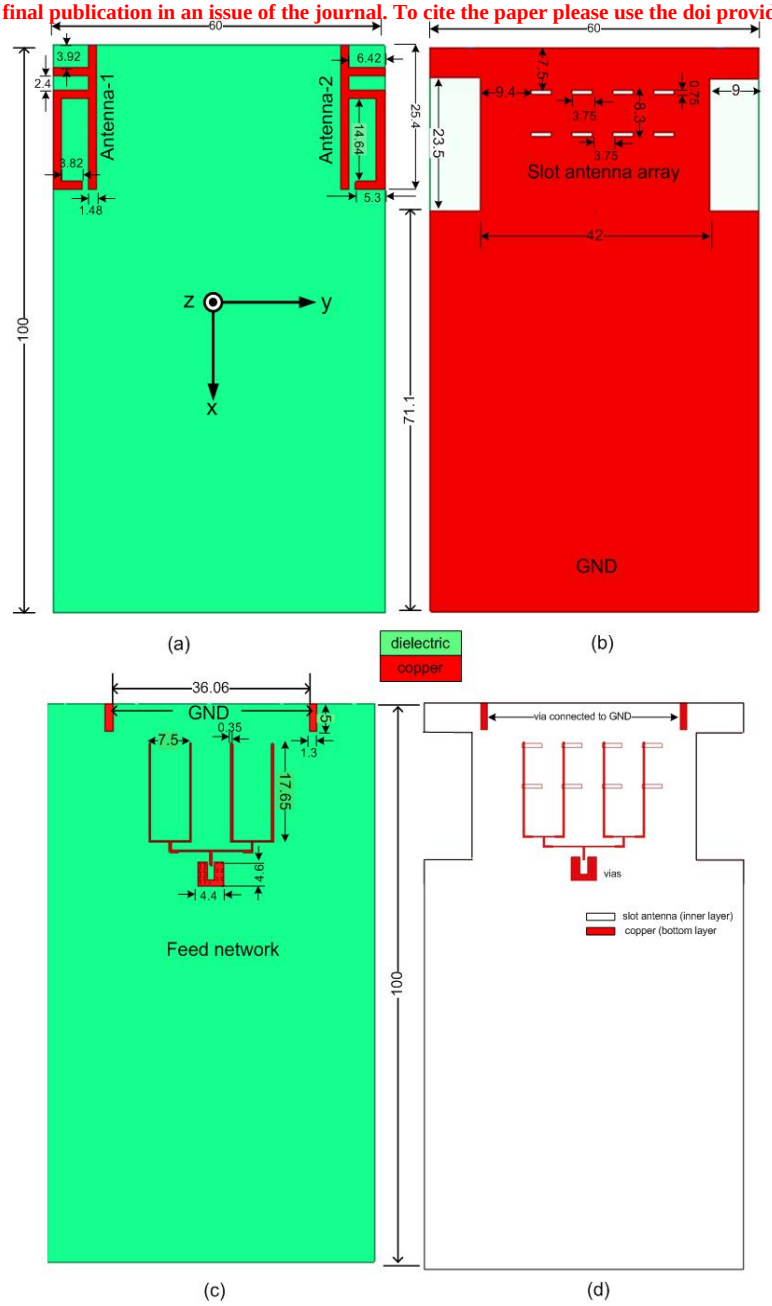

Figure 4: Dimensions in millimeters of the two-element 4G MIMO antenna (a), the ground plane layer with the mm-wave slot array (b), the mm-wave feed network (c), and the mm-wave 5G slot antenna array (with feeding network overlay).

The 0.13 mm-RO3003 substrate has the system ground plane on one end and the mm-wave array feed network on the other. Its ground side is glued to the top thick substrate holding the MIMO antenna system via a 0.05 mm substrate (prepreg), covering the slot antenna array as shown in Figure 4(b). Figure 4(d) shows the combination of two layers containing the slot antenna array and its feed network for better visualization. Although the mm-wave array is being fed with a corporate feed for broadside radiation, a switched beam feature can be added by utilizing a Butler matrix feed network. Such a network will occupy more space though for the added beam switching capability.

III. Simulation and Measurement Results

The complete integrated antenna system was modeled and simulated using HFSS^{TM}. The optimized design was fabricated using state of the art fabrication processes at Printech Labs, UK. The scattering parameters of the fabricated design were measured using an Agilent PNA-N5227A at King Fahd University for Petroleum and Minerals (KFUPM), Saudi Arabia. The gain patterns and efficiencies were measured at the Royal Military College (RMC), Canada and Microwave Vision Group (MVG), Italy, using a far field mm-wave setup and a SATIMO Starlab anechoic chamber, respectively. All measured and simulated results of the integrated MIMO antennas and mm-wave slot antenna arrays are summarized in the following subsections.

A. 4G MIMO Antenna Scattering Parameters

The simulated and measured reflection coefficients of the 2-element MIMO antenna system are shown in Figure 5(a) while the isolation curves are shown in Figure 5(b). Reflection coefficient measurements were made on two port for MIMO antennas while the third port was terminated with 50 Ω load. The wide-band MIMO antenna is resonating at a center frequency of 2160 MHz with a -6 dB impedance BW of 660 MHz. It can be observed that the MIMO antenna system covers frequency bands ranging from 1870 MHz to 2530 MHz. The measured isolation was more than 15 dB between the MIMO antennas and more than 25 dB between the MIMO antennas and the mm-wave array across the entire band of 4G/5G operation. Also, the measurements and simulations are in agreement. A slight difference in the simulated and measured results were observed because of the substrate properties, connector modeling and fabrication tolerances that are unavoidable. But such differences are minor and do not affect the behavior of the MIMO antenna system [8],[10].

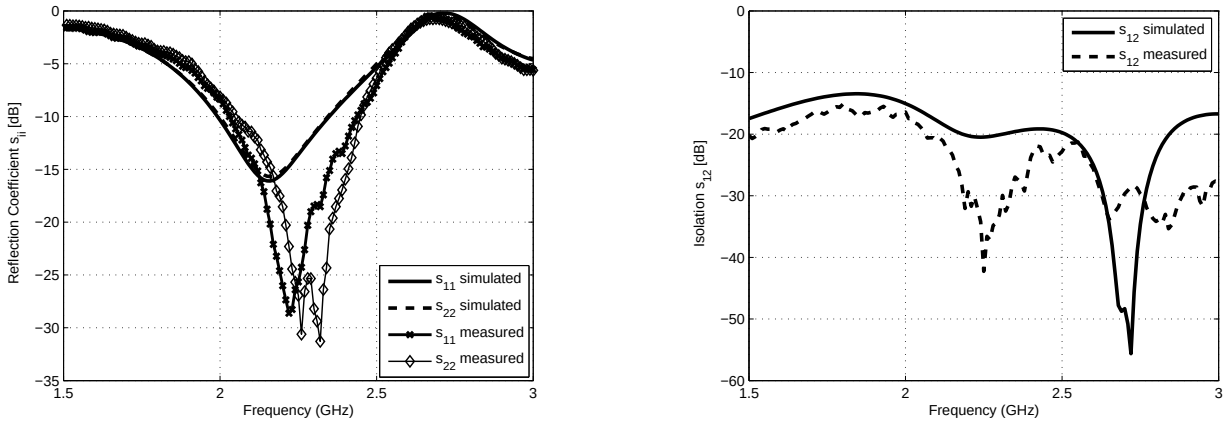

(a) (b)

Figure 5: (a) Reflection coefficients for the MIMO antenna system at its two ports (b) Isolation curves between the two MIMO antennas.

Antenna radiation efficiency and resonances are affected in the presence of a user hand and head especially in small antennas used in mobile handsets [3]. In [19], the head and hand influence were investigated in mobile handset antennas and suggested solutions to characterize it were provided. In practical designs, the placement of the radome will minimize such detuning.

B. mm-Wave Antenna Array Scattering Parameters

An important part of the mm-wave antenna array was the feeding netwrok. The feeding network was optimized to deliver maximum power at the output with minimum losses. Ideally, each output port should receive -6 dB power as each of the two power dividers halves the delivered power. The feeding network was simulated without the array in HFFS^{TM} to characterize its response. The amplitude and phase of the transmitted signals are shown in Figures 6(a) and 6(b), respectively. It shows the power received from input port-1 and their phases at each of the output port-k (k=2 to 5) in the frequency range from 27 GHz to 28.5 GHz. The output power at each of the four output ports was -6.369 dB, -6.279 dB, -6.008 dB and 6.261 dB with same phase at 28 GHz.

Figure 6(c) shows the simulated and measured reflection coefficients of the mm-wave array. The frequency bands covered (-10 dB reference level) were 26.8 to 28.4 GHz in simulation and 26.0 to 28.4 GHz in measurements. The simulation results were obtained without taking the effect of the mini-smp connector, soldering or fabrication tolerances. This can explain the slight difference between the measured and simulated curves. The measured S_{11} at 28 GHz covered the whole band of the simulated results showing good agreement. Such behavior is very common at very high frequency bands and has appeared in such mm-wave based antennas such as that in [20]–[22].

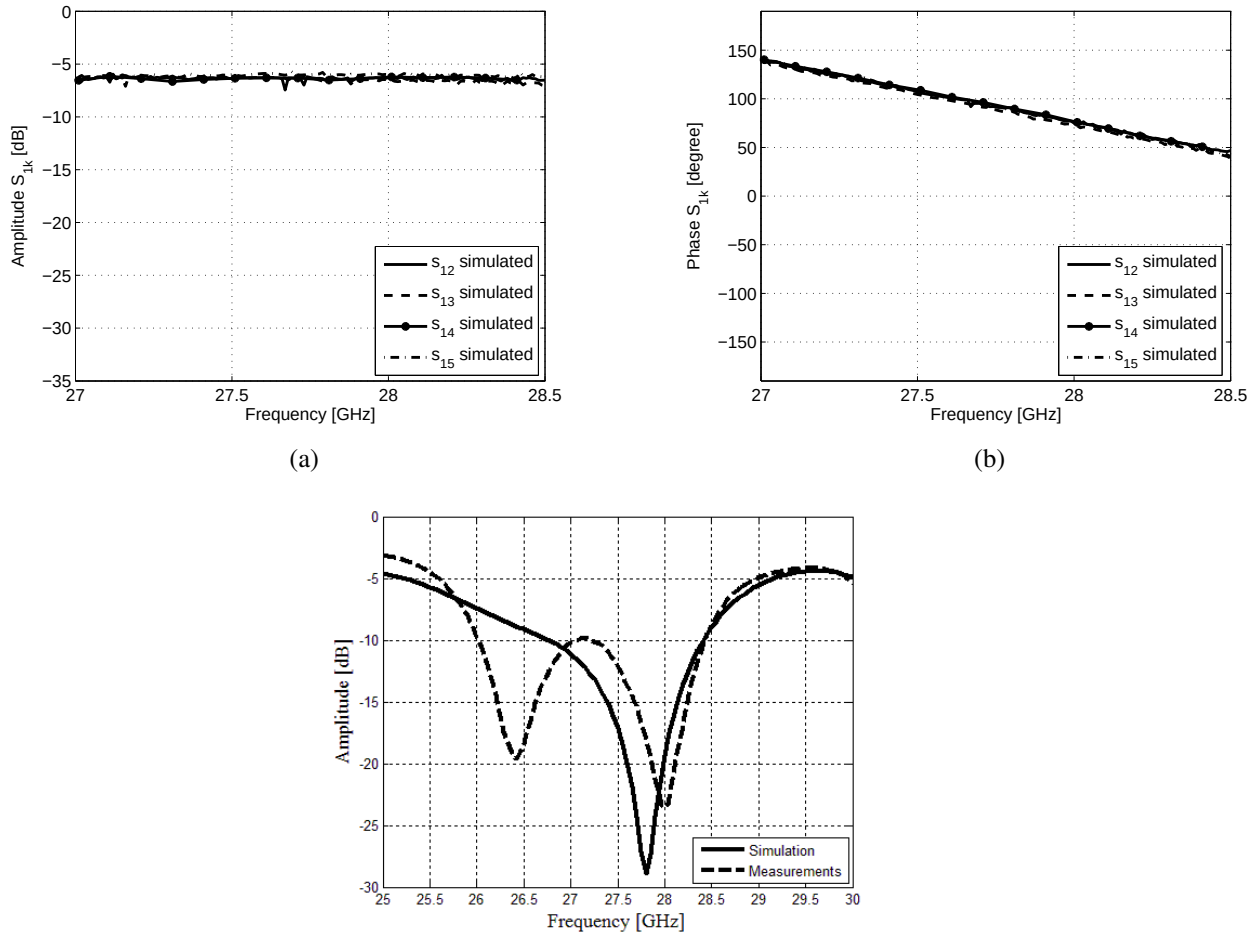

Figure 6: (a) Amplitude of transmission coefficients of the feednetwork (b) Phases of transmission coefficients of the feednetwork (c) Reflection coefficient versus frequency for the 5G mm-wave antenna array.

C. 4G MIMO Antenna Current Distribution

The MIMO antenna elements were further analyzed by studying the excited surface current densities using HFSS^{TM}. The goal of these simulations was to identify the resonant antenna parts and illustrate the amount of coupling between these elements. The analysis is shown at 2250 MHz and 2450 MHz in Figure 7. It shows the current density on the top surface antenna elements as well as the ground plane layer. Figures 7(a) and (b) show the current density when the rectangular path of current was activated at 2250 MHz while Figures 7(c) and (d) show the shorter straight line current path activated at 2450 MHz. As observed in these figures, a high current density was generated along the top side of the antenna elements while there was also some currents on the ground plane near each antenna element with reduced amplitude. This suggests that the ground plane is contributing to the radiation. Moreover, it is also noted that there is slight coupling between the two antenna elements.

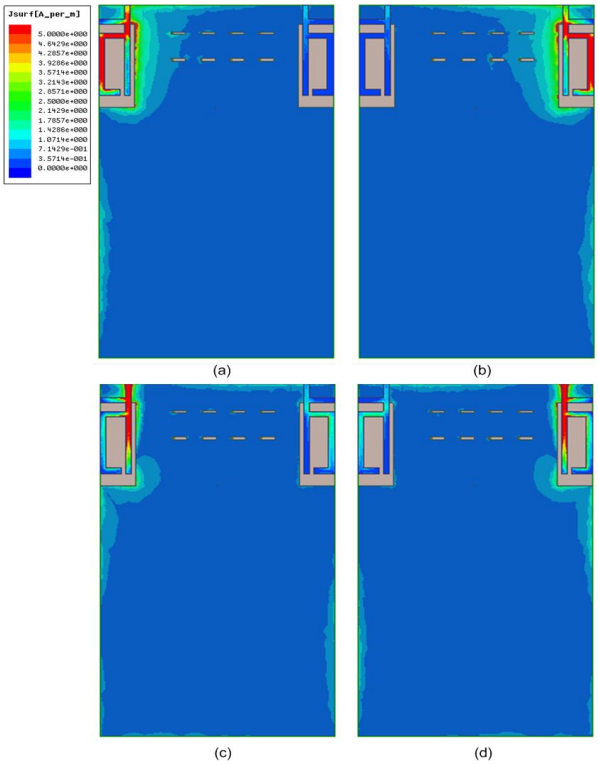

Figure 7: Current distribution for the MIMO antenna system: (a) Antenna-1 excited (2250 MHz), (b) Antenna-2 excited (2250 MHz), (c) Antenna-1 excited (2450 MHz), and (d) Antenna-2 excited (2450 MHz).

D. mm-Wave Antenna Array Current Distribution

The current distribution for the mm-Wave array is shown in Figure 8(a). The important thing to notice is that the current between the two slots is in phase and thus the patterns will add up in the far field, in addition, the magnitude difference between them was not exceeding 0.5 dB (the calculation was based on a microstrip line model ignoring the slot loading for a 1 λ inter-element spacing).

E. 4G MIMO Antenna Gain Patterns

The gain pattern measurement for the MIMO antenna system were carried out at the Microwave Vision Lab, Italy, using a SATIMO Starlab anechoic chamber. The measurement setup is shown in Figure 8(b).

The 3-dimensional (3-D) radiation patterns of the proposed MIMO antenna system were computed using HFSS^{TM}. The gain pattern for a single element was obtained when that element was excited while terminating the second element with a 50-Ω load. The simulated 3-D gain patterns were studied at three different frequencies which were 2.0 GHz, 2.25 GHz and 2.35 GHz; corresponding peak gain values were 4.13 dBi, 4.32 dBi and 4.39 dBi, respectively. The gain patterns for the two-element MIMO antenna are shown in Figures 9(a) and 9(b). The maxima of each element is tilted with respect to the other suggesting low field correlation which is desirable for MIMO operation.

The 2-D simulated and measured gain patterns for the MIMO antenna system are presented in Figures 9(c) and 9(d) at 2250 MHz. Figures 9(c) and 9(d) show the simulated and measured gain patterns for both antenna elements for their co-pol xz-plane and yz-plane, respectively. The pattern beam tilts are clear in Figure 9(d). For example, beam maximum are observed at $\pm 90^{\circ}$ for Antenna-1 and Antenna-2, respectively. In all measurements, one port was under investigation while the other was terminated with 50Ω load.

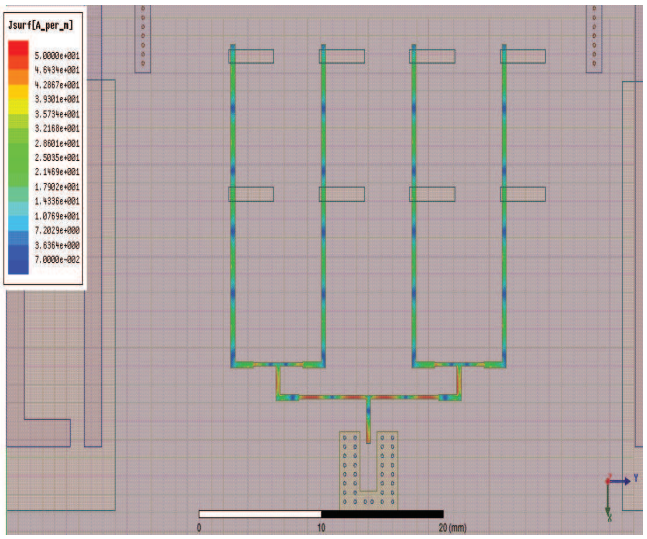

(a)

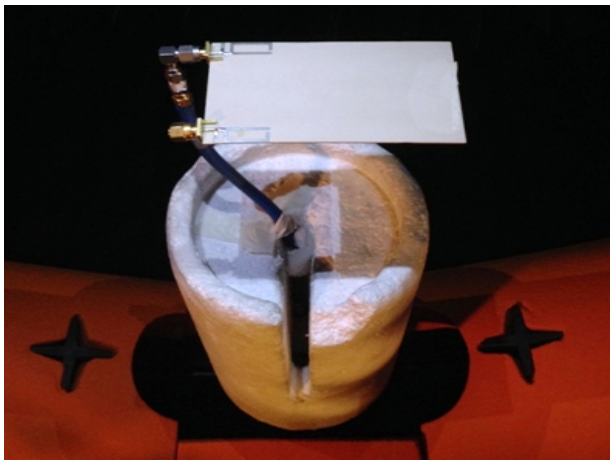

(b)

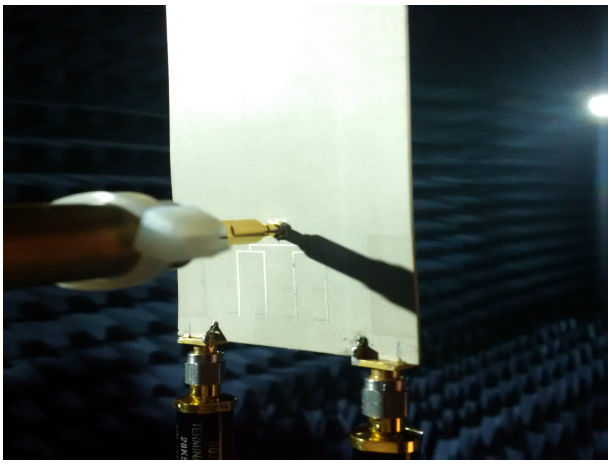

(c)

Figure 8: (a) Current distribution on the 5G mm-wave antenna array (b) Radiation pattern measurement setup for the 4G MIMO antenna system at microwave frequencies (c) Radiation pattern measurement setup for the mm-wave antenna array. The mini-smp connector (PE44489) for the mm-wave array is shown at antenna backside.

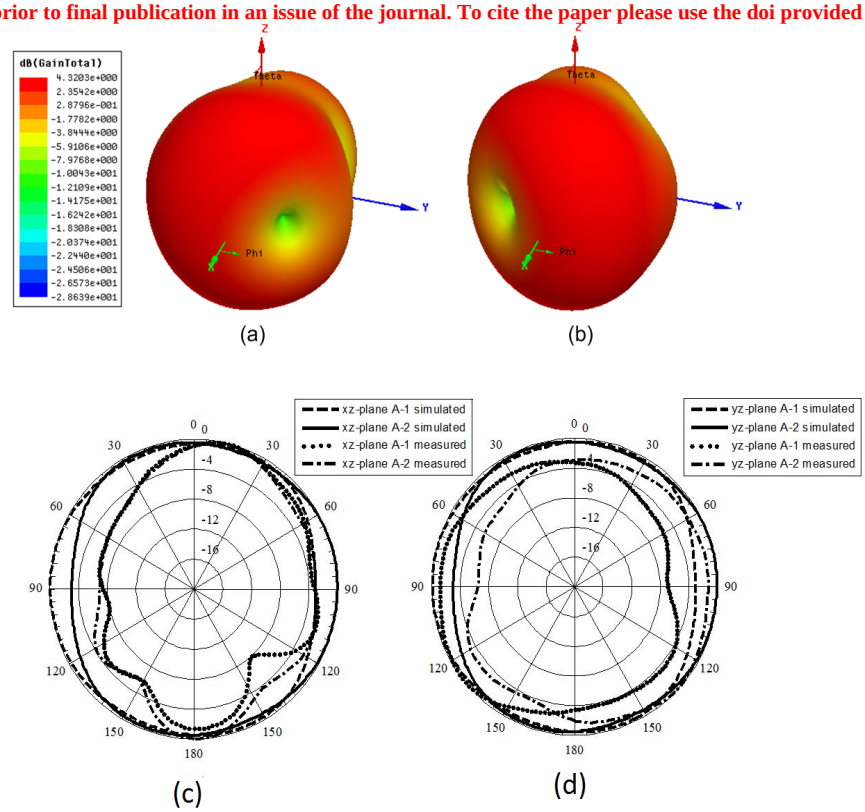

Figure 9: Simulated 3-D gain pattern at 2250 MHz for the 4G MIMO antenna:(a) antenna-1 (b) and antenna-2, Simulated and measured antenna beam patterns at 2250 MHz for the MIMO system: (c) xz-plane (Antenna-1, Antenna-2) (d) yz-plane (Antenna-1, Antenna-2)).

F. mm-wave Antenna Array Gain Patterns

The simulated realized gain of the mm-wave antenna array reached 9 dB at 28 GHz. The mm-wave array gain patterns were measured at The Royal Military College of Canada. The measurement setup is shown in Figure 8(c) and patterns are reported in Figures 10(a) and 10(b). Measured peak gain values were 8.2 dBi and results are in agreement with the simulations.

The difference between the measured and simulated curves in Figure 10(a) and 10(b) is due to the measurement setup and its limitation. The antenna mounting on the measurement setup blocked part of the back radiation that is shown in the simulations and not in the measurements. In addition, the measurements did not cover full 180 degrees, but rather almost ± 160 degrees. The simulated back lobe is large, indicating loss of energy in the head direction. This is inevitable, since we are using slot radiators. In a practical application, a metallic cover or another PCB with a GND plane for the LCD or something will block and reflect back most of this back radiation.

G. MIMO Antenna Characterization

MIMO antenna characterization is an essential part to qualify its operation. In this section, the proposed MIMO antenna system is characterized for its maximum gain, efficiency, correlation coefficient and the total active reflection coefficient (TARC).

For the given MIMO antenna system, the maximum gain and efficiency were also measured. The measurements were performed over a frequency band between 1.6 and 3 GHz as shown in Figure 10(c). The antenna performed very well in the desired frequency bands between 1.8 to 2.5 GHz. The efficiency of the antenna is more than 75% while the maximum gain is more than 3 dBi between 2.2 and 2.4 GHz.

The correlation coefficient (ρ) is an important parameter for MIMO antenna characterization. It is a measure of isolation among various MIMO channels. The calculation of ρ, based on the radiation patterns, shows the effect of various antenna elements operating simultaneously. For good MIMO operation, ρ should be less than 0.3. This value is the square root of the envelop correlation coefficient (ρ_e) which can be calculated in a uniform multipath environment using [3]:

$$\rho_e = \frac{|\int\int_{4\pi}[\vec{F_1}(\theta,\varphi) * \vec{F_2}(\theta,\varphi)d\Omega]|^2}{|\int\int_{4\pi}[\vec{F_1}(\theta,\varphi)|^2 d\Omega| \int\int_{4\pi}[\vec{F_2}(\theta,\varphi)|^2 d\Omega} \tag{1}$$

where $\vec{F_i}(\theta,\varphi)$ is the field radiation pattern of the antenna when port i is excited and $*$ denotes the Hermitian product. For the given MIMO antenna system, ρ_e was calculated at three distinct frequencies, 2.0 GHz, 2.25 GHz and 2.35 GHz, and the corresponding values were 0.1343, 0.1815, and 0.0058, respectively. It is clear that the given MIMO antenna system satisfies the requirement for good MIMO operation.

Total active reflection coefficient (TARC) is another metric for MIMO antenna systems and is defined as the ratio of the square root of the total reflected power divided by the square root of the total incident power in a multiport antenna system [3] and is given by:

$$\Gamma_a^t = \frac{\sqrt{\sum_{i=1}^{N} |b_i|^2}}{\sqrt{\sum_{i=1}^{N} |a_i|^2}} \tag{2}$$

where a_i and b_i are the incident signals and reflected signals, respectively.

TARC curves for the proposed MIMO antenna system are reported in Figure 10(d). The analysis was carried out by keeping the excitation of one port at $1e^{j0}$ while the phase of the second port was changed using different phase excitations. The TARC curves in Figure 10(d) are shown for excitation phases of 0^o, 30°, 60° and 90°. TARC curves also identify the effective operating BW of the MIMO antenna system. It is clear that the operating BW of the MIMO antenna system will not be affected by a phase change in the excitation of the other port.

IV. Conclusions

A novel integrated antenna system was presented complying with existing 4G wireless standards and upcoming 5G communication systems for broadband operation. The integrated solution consists of a microwave MIMO

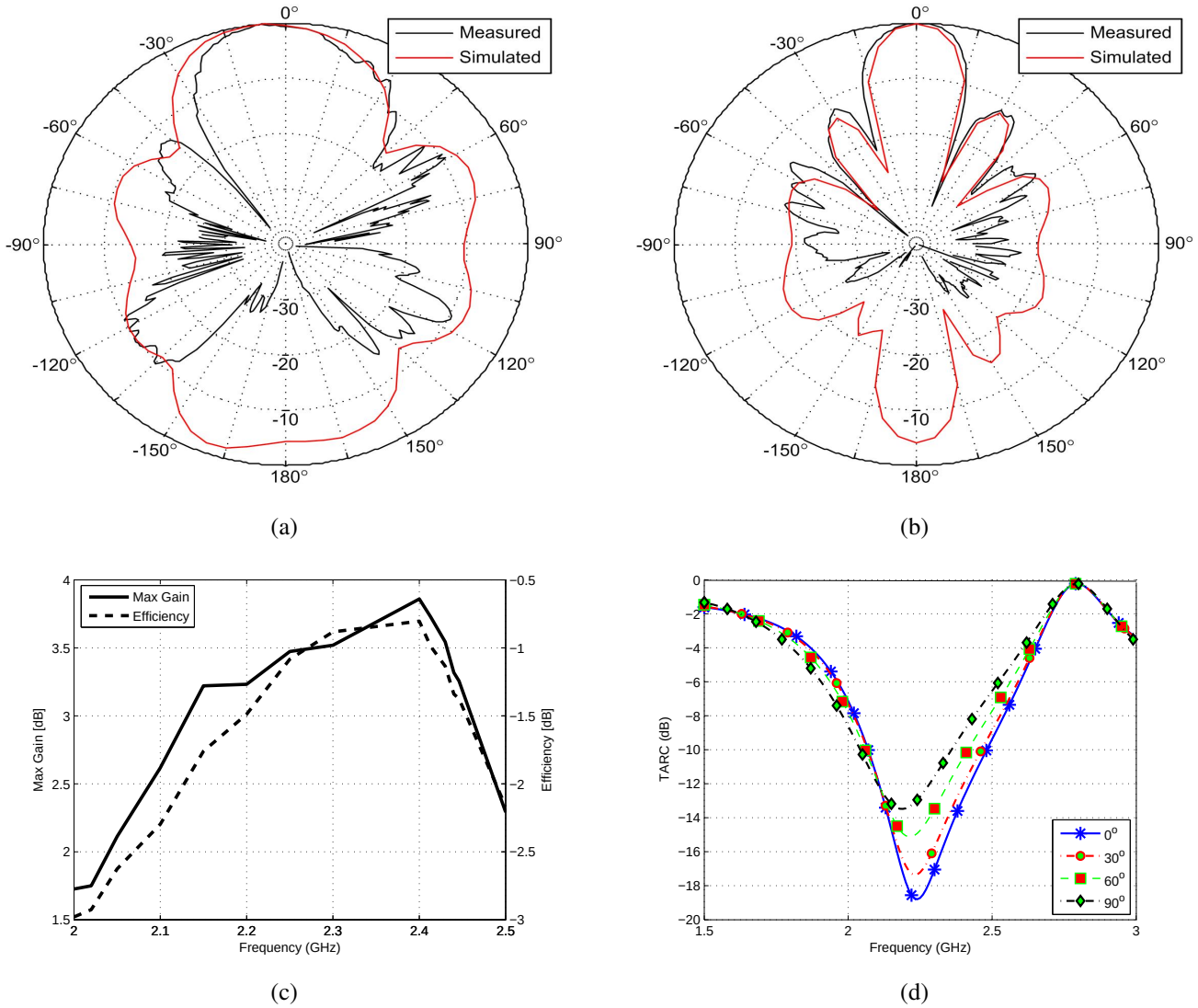

Figure 10: Measured and simulated gain patterns of the 5G mm-wave array at 28 GHz, (a) in the x-z plane, (b) y-z plane. Reduced accuracy in the measured patterns at backside (+90° to +270°) is possible due to interference effects of the rotating (metallic) antenna tower and the connecting cable. (c) Measured maximum gain and efficiency for the 4G MIMO antenna system. (d) TARC curves for the MIMO antenna system.

antenna embedded with a mm-wave slot antenna array with its feed network on the same multi-layer board. The compact microwave MIMO antenna covered a wide frequency band between 1870 to 2530 MHz while the mm-wave antenna array was designed to operate at 28 GHz with a minimum BW of 1.7 GHz. The antenna system was also characterized for MIMO parameters and offers suitable values in the desired band of operation. The maximum measured gain and the efficiency for the MIMO antenna system were 3.86 dBi and 83%, respectively.

The proposed system is well integrated and suited for existing 4G and upcoming 5G technology in wireless handheld devices and mobile terminals. The simple structure for the planar antenna elements also allow for practical

integration with other electronic circuitry.

ACKNOWLEDGMENTS

This work was supported by project number RG1423 through the Deanship of Scientific Research (DSR) at KFUPM, Dhahran, Saudi Arabia.

REFERENCES

[1] C.-X. Wang, F. Haider, X. Gao, X.-H. You, Y. Yang, D. Yuan, H. Aggoune, H. Haas, S. Fletcher, and E. Hepsaydir, "Cellular architecture and key technologies for 5g wireless communication networks," *Communications Magazine*, vol. 52, no. 2, pp. 122–130, 2014.

[2] M. S. Sharawi, "Printed multi-band mimo antenna systems and their performance metrics," *IEEE Antennas and Propagation Magazine*, vol. 55, pp. 218–232, 2013.

[3] ——, "Printed mimo antenna engineering," *Artech House*, 2014.

[4] Y. Yu, F. Jolani, and Z. Chen, "A wideband omnidirectional horizontally polarized antenna for 4g lte applications," *IEEE Antennas and Wireless Propagation Letter*, vol. 12, pp. 686–689, 2013.

[5] Y.-L. Ban, J.-H. Chen, J. L.-W. Li, and Y. Wu, "Small-size printed coupled-fed antenna for eight-band lte/gsm/umts wireless wide area network operation in an internal mobile handset," *IET Microwaves, Antennas & Propagation*, vol. 7, no. 6, pp. 399–407, 2013.

[6] M. E. de Cos, M. Mantash, A.-C. Tarot, and F. Las-Heras, "Dual-band coplanar waveguide-fed smiling monopole antenna for wifi and 4g long-term evolution applications," *IET Microwaves, Antennas & Propagation*, vol. 7, no. 9, pp. 777–782, 2013.

[7] N. I. M. Elamin, T. A. Rahman, and A. Y. Abdulrahman, "New adjustable slot meander patch antenna for 4g handheld devices," *Antennas and Wireless Propagation Letters, IEEE*, vol. 12, pp. 1077–1080, 2013.

[8] H. T. Chattha, M. Nasir, Q. H. Abbasi, Y. Huang, and S. S. Alja'afreh, "Compact low-profile dual-port single wideband planar inverted-f mimo antenna," *Antennas and Wireless Propagation Letters*, vol. 12, pp. 1673–1675, 2013.

[9] L. Sun, W. Huang, B. Sun, Q. Sun, and J. Fan, "Two-port pattern diversity antenna for 3g and 4g mimo indoor applications," *Antennas and Wireless Propagation Letters*, vol. 13, pp. 1573–1576, 2014.

[10] S. Roslan, M. R. Kamarudin, M. Khalily, and M. Jamaluddin, "An mimo rectangular dielectric resonator antenna for 4g applications," *Antennas and Wireless Propagation Letters, IEEE*, vol. 13, pp. 321–324, 2014.

[11] R. Hussain and M. S. Sharawi, "A cognitive radio reconfigurable mimo and sensing antenna system," *Antennas and Wireless Propagation Letters, IEEE*, vol. 14, pp. 257–260, 2015.

[12] ——, "An integrated reconfigurable mimo antenna system with an uwb sensing antenna for cognitive radio platforms," *IET Microwaves, Antennas & Propagation*, vol. 9, pp. 940–947, 2015.

[13] ——, "Planar 4-element frequency agile mimo antenna system with chassis mode reconfigurability," *Microwave and Optical Technology Letters*, vol. 57, pp. 1933–1938, 2015.

[14] T. S. Rappaport, S. Sun, R. Mayzus, H. Zhao, Y. Azar, K. Wang, G. N. Wong, J. K. Schulz, M. Samimi, and F. Gutierrez, "Millimeter wave mobile communications for 5g cellular: It will work!" *Access, IEEE*, vol. 1, pp. 335–349, 2013.

[15] T. S. Rappaport, F. Gutierrez, E. Ben-Dor, J. N. Murdock, Y. Qiao, J. Tamir *et al.*, "Broadband millimeter-wave propagation measurements and models using adaptive-beam antennas for outdoor urban cellular communications," *Antennas and Propagation, IEEE Transactions on*, vol. 61, no. 4, pp. 1850–1859, 2013.

[16] W. Hong, K. Baek, Y. Lee, and Y. G. Kim, "Design and analysis of a low-profile 28 ghz beam steering antenna solution for future 5g cellular applications," in *Microwave Symposium (IMS), 2014 IEEE MTT-S International*. IEEE, 2014, pp. 1–4.

[17] K.-S. Chin, H.-T. Chang, J.-A. Liu, H.-C. Chiu, J. S. Fu, and S.-H. Chao, "28-ghz patch antenna arrays with pcb and ltcc substrates," in *Cross Strait Quad-Regional Radio Science and Wireless Technology Conference (CSQRWC), 2011*, vol. 1. IEEE, 2011, pp. 355–358.

[18] K. Phalak, Z. Briquech, and A. R. Sebak, "Surface integrated waveguide fed antipodal fermi-linear tapered slot antenna at 28 ghz," in *16th International Symposium on Antenna Technology and Applied Electromagnetics (ANTEM)*. IEEE, 2014, pp. 1–2.

[19] C.-H. Li, E. Ofli, N. Chavannes, and N. Kuster, "Effects of hand phantom on mobile phone antenna performance," *IEEE Transactions on Antennas and Propagation*, vol. 57, no. 9, pp. 2763–2770, 2009.

[20] C.-H. Tseng, C.-J. Chen, and T.-H. Chu, "A low-cost 60-ghz switched-beam patch antenna array with butler matrix network," *IEEE Antennas and Wireless Propagation Letters*, vol. 7, pp. 432–435, 2008.

[21] Moulder, William F and Khalil, Waleed and Volakis, John L, "60-GHz two-dimensionally scanning array employing wideband planar switched beam network," *IEEE Antennas and Wireless propagation letters*, vol. 9, pp. 818–821, 2010.

[22] Patterson, Chad E and Khan, Wasif Tanveer and Ponchak, George E and May, Gary S and Papapolymerou, John, "A 60-GHz active receiving switched-beam antenna array with integrated butler matrix and GaAs amplifiers," *IEEE Transactions on Microwave Theory and Techniques*, vol. 60, no. 11, pp. 3599–3607, 2012.